Engineering Science and Technology, an International Journal xxx (2018) xxx–xxx

HOSTED BY

ELSEVIER

Contents lists available at ScienceDirect

Engineering Science and Technology, an International Journal

journal homepage: www.elsevier.com/locate/jestch

Full Length Article

Modelling and analysis of dual stator-winding induction machine using complex vector approach

A.S.O. Ogunjuyigbe, T.R. Ayodele *, B.B. Adetokun

Power, Energy, Machines and Drives (PEMD) Research Group, Electrical and Electronic Engineering Department, Faculty of Technology, University of Ibadan, Nigeria

ARTICLE INFO

Article history:
Received 3 March 2017
Revised 14 March 2018
Accepted 24 March 2018
Available online xxxx

Keywords:
Complex vector
Modelling
Simulation
Dual stator
Induction machine
MATLAB-Simulink

ABSTRACT

In this work, complex vector modelling technique is utilized to develop and simulate a dual stator-winding induction machine with squirrel-cage rotor. The transient and dynamic performances of the machine under two cases of input conditions are analysed and presented both at no load and when a constant load torque is applied. The modelling and simulation has been carried out in a step-wise procedure that clearly set forth for the complex vector Simulink implementation in a MATLAB-Simulink environment. The approach presented in this work can easily be applied to other types and configurations of electric machines and drives.

1. Introduction

The concept of dual-stator-winding machines and its applications has gained prominence in recent years [1–4]. Two categories of these machines have been identified [5]. The first is the split-wound dual-stator winding machine designed to increase power capabilities of large synchronous generator. The second category is the brushless doubly fed machine (BDFM), also known as self-cascaded machine, is made up of 3-phase windings embedded in a common stator structure and a special rotor structure which allow the effects of cascade connection through the nested loops on the rotor.

The dual stator machines find applications in several systems, ranging from synchronous machines with AC and DC outputs to large pumps, compressors and rolling mills driven by induction motors. A new dual-stator-winding squirrel cage induction machine was proposed in [6]. It consists of two separate symmetrical 3-phase windings embedded in the same stator structure but wound to have unequal number of poles in the ratio $1:3$. The rotor structure is a standard squirrel cage rotor with skewed rotor bars, which is intended to reduce the magnitude of harmonic torques due to the harmonic content of the magneto motive force (MMF) waves [7]. Fig. 1 shows the dual stator winding distributions of a typical induction machine [6].

This design eliminates the circulating harmonic currents and the net magnetic coupling between the two windings of the stator. It has been shown that the best configuration is $2poles - 6poles$ structure. The output torque is the algebraic sum of two independent torques developed by the independent interaction of each stator current with the rotor flux. With these two independent torques, the machine can be easily operated at high/medium speed and at low speed, when the torques are added and subtracted respectively. Such dual stator machine behaves like two independent induction machines mechanically coupled through the shaft, due to the decoupling effect produced by the dissimilar pole pairs, whereupon all the control schemes for induction machine can also be applied to the dual stator winding machine [6].

Some work have been presented on the dual stator-winding machines in the literature: Pienkowski [8] developed mathematical models of dual stator squirrel-cage induction motor, formulated in phase coordinate system. The author considered the control systems of field-oriented control and direct torque control for the induction motor. Similarly, Dehghanzadeh and Behjat [9] have developed a dynamic model of a dual-stator permanent magnet synchronous generator using a technique that could transform two stator winding sets to two winding couples on the d-q axes of the rotor reference frame. Bu et al. [10] have presented slip frequency control strategy and its experimental implementation of dual-stator-winding induction generator for variable frequency

* Corresponding author.
E-mail addresses: a.ogunjuyigbe@ui.edu.ng (A.S.O. Ogunjuyigbe), tr.ayodele@ui.edu.ng (T.R. Ayodele).

Peer review under responsibility of Karabuk University.

https://doi.org/10.1016/j.jestch.2018.03.013
2215-0986/© 2018 Karabuk University. Publishing services by Elsevier B.V.

Please cite this article in press as: A.S.O. Ogunjuyigbe et al., Modelling and analysis of dual stator-winding induction machine using complex vector approach, Eng. Sci. Tech., Int. J. (2018), https://doi.org/10.1016/j.jestch.2018.03.013

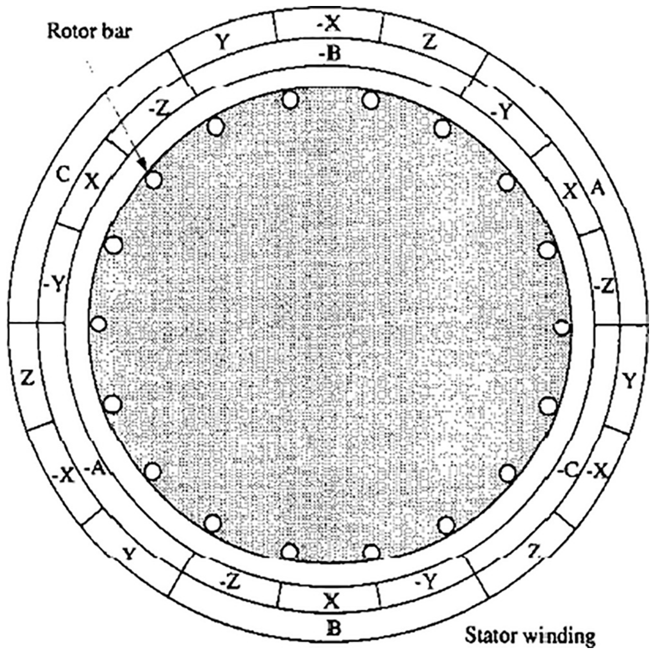

Fig. 1. Dual Stator Winding Distributions.

generating system. The generator has two sets of stator windings embedded into the stator slots. The power winding produces the variable frequency AC power to feed the loads, and the control winding was connected to the static excitation controller to control the generator for output voltage regulation with speed and load variations. Slimene et al. [11] have examined a steady state performance analysis of stand-alone double stator induction generator self-excited with two independents capacitors banks. An impedance approach based on double three-phase induction-generator model was employed to derive steady equations of the double stator self-excited Induction generator. In another work, Slimene et al. [12] modelled and analysed self-excited dual stator winding induction generator (DSWIG) using fzero algorithm. A prototype of the dual stator-winding induction generator (DWIG) and its dynamic model to verify the validity of this machine design as variable speed generator for renewable energy systems has been presented by Rodrigo et al. [13]. The authors revealed that the proposed DWIG has a better use of energy compared to a squirrel cage induction generator (SCIG) in variable speed applications. It was also revealed that the performance of DWIG with a bidirectional converter is very similar to those described in other studies with brushless doubly-fed induction generators. An optimized design using efficiency as the objective function of a dual stator winding induction generator with standard squirrel cage rotor for wind turbine applications was proposed by Keshtkar and Zarchi. The authors determined the optimal parameter values for the machine and then evaluated the machine using the finite-element method supported by Ansys Maxwell software. Their result revealed that a significant efficiency (3 times) was achieved with the optimized dual stator winding induction generator compared to conventional design. Amimeur et al. [14] has presented the detailed modelling of a dual-stator windings of self-excited induction generator in synchronous reference frame. The authors considered the effects of common mutual leakage inductance between two three-phase windings sets. The dynamics of self-excitation process, and step application of load on the machine were also presented. Similarly, Hamoud et al. [15] presented a systematic modelling, a detailed analysis and the performance analysis of self-excitation dual stator winding induction generator. The modelling of the generator took into consideration the common mutual leakage inductance between stators and the magnetizing inductance, which played a principal role in the stabilization of the output voltage in the steady state.

Complex vector modelling has also been applied in recent years. For example, Mu~noz and Lipo [16] presented a new detailed mathematical derivation of a squirrel-cage induction machine d–q model. The model was based on coupled magnetic circuit theory and complex space-vector notation which took into account the actual non-sinusoidal rotor bar distribution. It was shown that, given the structural symmetry of the induction machine, both stator and rotor circuits could be modelled by the simple set of only four coupled differential equations. The actual *n* rotor bars and end-ring currents were fully included in the model, and they were obtained directly by using a simple vector transformation. In another work, Wu, and Ojo [5] ultilised the winding-function method to calculate the inductances in induction machine. In their work, the phase-voltage and torque equations were transformed to the rotor reference frame to facilitate simplicity of modelling and using an *n/spl times/n* complex-variable reference frame transformation.

Most of the aforementioned authors have done well in modelling, simulating and analysing dual-stator winding machines, However, conventional modelling approach were adopted in most of the models. In this work, the dual-stator winding induction machine is modelled and simulated using complex vector notations. The developed model allows the computation of the rotor-bar currents. Unlike the conventional induction machine whereby both the stator and the rotor are modelled as 3-phase systems, the rotor is here modelled as an n-phase system, where n is the number of rotor bars. This analysis therefore requires complex transformation in order to obtain each rotor bar current. This method has been employed for the modelling of single stator-winding squirrel cage induction machine in [16,17].

2. Mathematical modelling of dual Stator-winding induction Machine using complex vector

In modelling the dual stator-winding induction machine, the following general assumptions have been made: (i) uniform air gap, (ii) negligible saturation, (iii) sinusoidal distribution of stator windings, (iv) naturally isolated stator windings and (v) negligible inter-bar current. In this paper, complex vector representation has been used both for the modelling and the simulation in MATLAB-Simulink.

2.1. Stator voltage equations

The stator voltage equations in machine variables may be expressed as

$$v_{abc} = r_{abc} i_{abc} + p\lambda_{abc} \Rightarrow v_{s1} = r_{s1} i_{s1} + p\lambda_{s1} \tag{1}$$

$$v_{xyz} = r_{xyz} i_{xyz} + p\lambda_{xyz} \Rightarrow v_{s2} = r_{s2} i_{s2} + p\lambda_{s2} \tag{2}$$

$$f_{s1} = [f_{as} f_{bs} f_{cs}]^T \tag{3}$$

$$f_{s2} = [f_{xs} f_{ys} f_{zs}]^T \tag{4}$$

where *f* represents voltage, current and flux linkage vector. The subscripts s_1 and s_2 denote variables and parameters associated with the first (abc) and the second (xyz) stator windings respectively; $\boldsymbol{r_{s1}}$ and $\boldsymbol{r_{s2}}$ are the diagonal 3×3 resistance matrices for abc and xyz stator windings respectively.

In complex vector variable form (1) and (2) can be written as [18]:

Please cite this article in press as: A.S.O. Ogunjuyigbe et al., Modelling and analysis of dual stator-winding induction machine using complex vector approach, Eng. Sci. Tech., Int. J. (2018), https://doi.org/10.1016/j.jestch.2018.03.013

$$\underline{v}_{s1} = r_{s1}\underline{i}_{s1} + p\underline{\lambda}_{s1} \tag{5}$$

$$\underline{v}_{s2} = r_{s2}\underline{i}_{s2} + p\underline{\lambda}_{s2} \tag{6}$$

The complex vector arbitrary variables $\underline{f}_{s1}$ and $\underline{f}_{s2}$ are given by

$$\underline{f}_{s1} = \frac{2}{3}(f_{as} + \underline{a}f_{bs} + \underline{a}^2 f_{cs}) \tag{7}$$

$$\underline{f}_{s2} = \frac{2}{3}(f_{xs} + \underline{a}f_{ys} + \underline{a}^2 f_{zs}) \tag{8}$$

where $\underline{a} = e^{j\frac{2\pi}{3}}$ and $\boldsymbol{f}$ denotes voltage, current and flux linkages.

2.2. Stator Flux-linkage equations

The flux-linkage of each stator winding may be written as the combination of three flux-linkage components as follows:

$$\lambda_{s1} = \lambda_{s1s1} + \lambda_{s1s2} + \lambda_{s1r} \tag{9}$$

Where λ_{s1s1} represents the abc stator-winding flux linkages due only to the current flowing in it; λ_{s1s2} denotes the flux-linkages due to the current flowing in the xyz stator winding and $\lambda_{s1r\ r}$ is the flux-linkages as a result of the rotor currents.

Similarly,

$$\lambda_{s2} = \lambda_{s2s2} + \lambda_{s2s1} + \lambda_{s2r} \tag{10}$$

Due to the decoupling effect of the difference in pole number of the machine, the mutual inductances between the two windings are zero, whereupon

$$\lambda_{s1s2} = \lambda_{s2s1} = 0 \tag{11}$$

also, the mutual leakage inductances (and hence flux linkages) has been clearly shown in [6] to be zero. Thus Eqs. (9) and (10) reduces to:

$$\lambda_{s1} = \lambda_{s1s1} + \lambda_{s1r} \tag{12}$$

$$\lambda_{s2} = \lambda_{s2s2} + \lambda_{s2r} \tag{13}$$

In matrix form,

$$\begin{bmatrix}\lambda_{s1}\\ \lambda_{s2}\end{bmatrix} = \begin{bmatrix}L_{s1} & 0\\ 0 & L_{s2}\end{bmatrix}\begin{bmatrix}i_{s1}\\ i_{s2}\end{bmatrix} + \begin{bmatrix}L_{s1r} & 0\\ 0 & L_{s2r}\end{bmatrix}\begin{bmatrix}i_{r1}\\ i_{r2}\end{bmatrix} \tag{14}$$

where

$$L_{si} = \begin{bmatrix}L_{lsi}+L_{msi} & -L_{msi}/2 & -L_{msi}/2\\ -L_{msi}/2 & L_{lsi}+L_{msi} & L_{lsi}+L_{msi}\\ L_{lsi}+L_{msi} & -L_{msi}/2 & L_{lsi}+L_{msi}\end{bmatrix}; \text{for} \quad i = 1,2 \tag{15}$$

L_{s1r} and L_{s2r} are given by [2]

$$L_{s1r} = \begin{bmatrix}L_{a1} & L_{a2} & \dots & L_{a(n-1)} & L_{an}\\ L_{b1} & L_{b2} & \dots & L_{b(n-1)} & L_{bn}\\ L_{c1} & L_{c2} & \dots & L_{c(n-1)} & L_{cn}\end{bmatrix} \tag{16}$$

$$L_{s2r} = \begin{bmatrix}L_{x1} & L_{x2} & \dots & L_{x(n-1)} & L_{xn}\\ L_{y1} & L_{y2} & \dots & L_{y(n-1)} & L_{yn}\\ L_{z1} & L_{z2} & \dots & L_{z(n-1)} & L_{zn}\end{bmatrix} \tag{17}$$

where $L_{a(x)i}$ is the mutual inductance between the phase *a(x)* and the *ith* rotor loop; $L_{b(y)i}$ is the mutual inductance between the phase *b(y)* and the *ith* rotor loop; $L_{c(z)i}$ is the mutual inductance between the phase *c(z)* and the *ith* rotor loop.

In complex vector variable form, (14) can be written as

$$\underline{\lambda}_{s1} = L_{s1}\underline{i}_{s1} + L_{s1r}\underline{i}_{r1} \tag{18}$$

$$\underline{\lambda}_{s2} = L_{s2}\underline{i}_{s2} + L_{s2r}\underline{i}_{r2} \tag{19}$$

It can be shown that L_{si} in (18) and (19) is [18]:

$$L_{si} = L_{lsi} + \frac{3}{2}L_{msi} \tag{20}$$

$$L_{sir} = \frac{n}{2}L_{mi}e^{jp_i(\theta_r+\delta)} \tag{21}$$

where

$$L_{mi} = \frac{4\sin p_i\delta}{\pi N_{si}}L_{msi} \tag{22}$$

p_i is the number of pole pairs for $i = 1, 2$ and δ is half the angle between two adjacent rotor bars.

The complex vector rotor currents are defined as:

$$\underline{i}_{ri} = \frac{2}{n}\begin{bmatrix}1 & \underline{b}^{p_i} & \underline{b}^{2p_i} & \cdots & \underline{b}^{(n-1)p_i}\end{bmatrix}\begin{bmatrix}i_{r1}\\ i_{r2}\\ \vdots\\ i_{r(n-1)}\\ i_{rn}\end{bmatrix}; i = 1,2 \tag{23}$$

where $\underline{b} = exp(j2\pi/n)$

The column vector in the RHS of (23) denotes the instantaneous rotor loop currents.we can thus write (18) and (19) as follows:

$$\underline{\lambda}_{s1} = \left(L_{ls1} + \frac{3}{2}L_{ms1}\right)\underline{i}_{s1} + \frac{n}{2}L_{m1}e^{jp_1(\theta_r+\delta)}\underline{i}_{r1} \tag{24}$$

$$\underline{\lambda}_{s2} = \left(L_{ls2} + \frac{3}{2}L_{ms2}\right)\underline{i}_{s2} + \frac{n}{2}L_{m2}e^{jp_2(\theta_r+\delta-\xi)}\underline{i}_{r2} \tag{25}$$

where ξ is the arbitrary angle of displacement between the two stator windings, which may be zero.

We can now substitute (24) and (25) into (5) and (6), and after differentiation using product rule, we have:

$$\underline{v}_{s1} = r_{s1}\underline{i}_{s1} + \left(L_{ls1} + \frac{3}{2}L_{ms1}\right)p\underline{i}_{s1} + \frac{n}{2}L_{m1}e^{jp_1(\theta_r+\delta)}(p + jp_1\omega_r)\underline{i}_{r1} \tag{26}$$

$$\underline{v}_{s1} = r_{s2}\underline{i}_{s2} + \left(L_{ls2} + \frac{3}{2}L_{ms2}\right)p\underline{i}_{s2} + \frac{n}{2}L_{m2}e^{jp_2(\theta_r+\delta-\xi)}(p + jp_2\omega_r)\underline{i}_{r2} \tag{27}$$

2.3. Rotor voltage equation

The squirrel cage rotor voltage equation in machine variables may be briefly written in complex vector notation as

$$\underline{0} = r_r\underline{i}_r + p\underline{\lambda}_r \tag{28}$$

Where r_r is the rotor resistance matrix and $\underline{\lambda}_r$ is the rotor loop flux linkage complex vector. Equation (28) may be writen in matrix form as:

$$\begin{bmatrix}0\\ 0\\ \vdots\\ 0\end{bmatrix} = \begin{bmatrix}2(r_b+r_e) & -r_b & \cdots & -r_b\\ -r_b & 2(r_b+r_e) & \cdots & 0\\ \vdots & \vdots & \ddots & \vdots\\ -r_b & 0 & \cdots & 2(r_b+r_e)\end{bmatrix}\begin{bmatrix}i_{r1}\\ i_{r2}\\ \vdots\\ i_{rn}\end{bmatrix} + p\begin{bmatrix}\lambda_{r1}\\ \lambda_{r2}\\ \vdots\\ \lambda_{rn}\end{bmatrix} \tag{29}$$

We can thus write the kth rotor loop voltage equation as

$$0 = -r_b i_{r(k-1)} + 2(r_b + r_e)i_{r(k)} - r_b i_{r(k+1)} + p\lambda_{rk} \tag{30}$$

2.4. Rotor Flux-linkage equations

The total rotor flux linkages may be written as the combination of three components:

$$\lambda_r = \lambda_{rr} + \lambda_{rs1} + \lambda_{rs2} \tag{31}$$

The first flux linkage component is due to the rotor currents, the second and third are due to the *abc* and *xyz* stator winding currents respectively.

In complex vector form, the total rotor flux linkage in the p_1 pole pair winding subspace is written as [6]:

$$\underline{\lambda}_{r1} = L_{r1}\underline{i}_{r1} + \frac{3}{2}L_{m1}e^{-jp_1(\theta_r+\delta)}\underline{i}_{s1} \tag{32}$$

Similarly, the total rotor flux linkage in the p_2 pole pair winding subspace is

$$\underline{\lambda}_{r2} = L_{r2}\underline{i}_{r2} + \frac{3}{2}L_{m2}e^{-jp_2(\theta_r+\delta-\xi)}\underline{i}_{s2} \tag{33}$$

Putting (32) and (33) respectively into (28) and after differentiating using product rule, the rotor voltage equations can thus be written as:

$$\underline{0} = r_{r1}\underline{i}_{r1} + L_{r1}p\underline{i}_{r1} + \frac{3}{2}L_{m1}e^{-jp_1(\theta_r+\delta)}(p - jp_1\omega_r)\underline{i}_{s1} \tag{34}$$

$$\underline{0} = r_{r2}\underline{i}_{r2} + L_{r2}p\underline{i}_{r2} + \frac{3}{2}L_{m2}e^{-jp_2(\theta_r+\delta-\xi)}(p - jp_2\omega_r)\underline{i}_{s2} \tag{35}$$

The equivalent rotor resistances and inductances in the p_i pole pair subspace are respectively expressed as:

$$r_{ri} = 2R_e + 2R_b[1 - \cos(p_i\alpha_r)] \tag{36}$$

$$L_{ri} = 2L_e + 2L_b[1 - \cos(p_i\alpha_r)] + \frac{\mu_\circ lr}{g}(p_i\alpha_r) \tag{37}$$

where i = 1, 2

2.5. Complex vector reference frame transformation

The equations written so far are in terms of the machine variables. Transformation of variables is often needed in order to eliminate time-varying inductances thereby simplifying the machine models and affording ease of computation and simulation.

Complex vector transformation from machine variables into *dq* variables for the stator may be generally defined by [18]:

$$\underline{f}_{qds} = \frac{2}{3}e^{-j\theta}[f_{as} + \underline{a}f_{bs} + \underline{a}^2 f_{cs}] = e^{-j\theta}\underline{f}_{abcs} \tag{38}$$

Where the angular displacement of the reference frame, θ is defined as

$$\theta = \int \omega(t)dt + \theta(0) \tag{39}$$

$\theta(0)$ is the initial condition of θ .

The transformation for the n-phase rotor system may be written as [19]:

$$\underline{i}_{qdr} = \frac{2}{3}\sqrt{\frac{3}{n}}e^{-j(\theta_1-\theta_r-\delta)}\underline{i}_r \tag{40}$$

Applying the transformation in (38) and (40) in the stator and rotor voltage equations in (28), (29); and (34), (35) respectively, the complex vector voltage equations in arbitrary reference frame can thus be expressed as:

$$\underline{v}_{qds1} = r_{s1}\underline{i}_{qds1} + jp_1\omega_1\underline{\lambda}_{qds1} + p\underline{\lambda}_{qds1} \tag{41}$$

$$\underline{v}_{qds2} = r_{s2}\underline{i}_{qds2} + jp_2\omega_2\underline{\lambda}_{qds2} + p\underline{\lambda}_{qds2} \tag{42}$$

$$\underline{0} = r_{r1}\underline{i}_{qdr1} + jp_1(\omega_1 - \omega_r)\underline{\lambda}_{qdr1} + p\underline{\lambda}_{qdr1} \tag{43}$$

$$\underline{0} = r_{r2}\underline{i}_{qdr2} + jp_2(\omega_2 - \omega_r)\underline{\lambda}_{qdr2} + p\underline{\lambda}_{qdr2} \tag{44}$$

where

$$\underline{\lambda}_{qds1} = (L_{s1} - L'_{m1})\underline{i}_{qds1} + L'_{m1}(\underline{i}_{qds1} + \underline{i}_{qdr1}) = L_{s1}\underline{i}_{qds1} + L'_{m1}\underline{i}_{qdr1} \tag{45}$$

$$\underline{\lambda}_{qds2} = (L_{s2} - L'_{m2})\underline{i}_{qds2} + L'_{m2}(\underline{i}_{qds2} + \underline{i}_{qdr2}) = L_{s2}\underline{i}_{qds2} + L'_{m2}\underline{i}_{qdr2} \tag{46}$$

$$\underline{\lambda}_{qdr1} = (L_{r1} - L'_{m1})\underline{i}_{qdr1} + L'_{m1}(\underline{i}_{qdr1} + \underline{i}_{qds1}) = L_{r1}\underline{i}_{qdr1} + L'_{m1}\underline{i}_{qds1} \tag{47}$$

$$\underline{\lambda}_{qdr2} = (L_{r2} - L'_{m2})\underline{i}_{qdr2} + L'_{m2}(\underline{i}_{qdr2} + \underline{i}_{qds2}) = L_{r2}\underline{i}_{qdr2} + L'_{m2}\underline{i}_{qds2} \tag{48}$$

The *qd* complex vector equivalent circuit of the dual stator winding squirrel cage induction machine is shown in Fig. 2.

2.6. Torque equation

For a linear magnetic circuit, the electromagnetic torque for a *P-pole* machine is generally defined mathematically as the partial derivative of the coenergy, W_c with respect to the mechanical angular displacement of the rotor θ_{rm}. That is [7]:

$$T_e = \frac{\partial W_c}{\partial \theta_{rm}} = \left(\frac{p}{2}\right)\frac{\partial W_c}{\partial \theta_r} \tag{49}$$

where

$$\theta_r = \left(\frac{p}{2}\theta_{rm}\right) \tag{50}$$

The total elecromagnetic torque developed by the dual stator winding induction machine is the algebraic sum of each torque produced separately by the interaction of each stator winding with the rotor. Thus, the electromagnetic torque for the machine can be expressed as

$$T_e = p_1 i_{s1}^T \frac{\partial}{\partial \theta_r}[L_{sr1}]i_r + p_2 i_{s2}^T \frac{\partial}{\partial \theta_r}[L_{sr2}]i_r \tag{51}$$

$[L_{sr1}]$ and $[L_{sr2}]$ are the matrices of the mutual inductances between each stator and rotor circuits respectively and they can be expressed as [19]:

$$L_{sr1} = \frac{L_{m1}}{2}\left\{\begin{matrix} e^{jp_1(\theta_r+\delta)}\begin{bmatrix}1\\ a^2\\ a\end{bmatrix}\begin{bmatrix}1 & b & \cdots & b^{n-1}\end{bmatrix}+ \\ e^{-jp_1(\theta_r+\delta)}\begin{bmatrix}1\\ a\\ a^2\end{bmatrix}\begin{bmatrix}1 & b^{-1} & \cdots & b^{1-n}\end{bmatrix}\end{matrix}\right\} \tag{52}$$

$$L_{sr2} = \frac{L_{m2}}{2}\left\{\begin{matrix} e^{jp_2(\theta_r+\delta-\xi)}\begin{bmatrix}1\\ a^2\\ a\end{bmatrix}\begin{bmatrix}1 & b & \cdots & b^{n-1}\end{bmatrix}+ \\ e^{-jp_2(\theta_r+\delta-\xi)}\begin{bmatrix}1\\ a\\ a^2\end{bmatrix}\begin{bmatrix}1 & b^{-1} & \cdots & b^{1-n}\end{bmatrix}\end{matrix}\right\} \tag{53}$$

Substituting (52) and (53) into (51), the torque can thus be expressed in terms of qd variables as

$$\begin{aligned} T_e = {} & p_1\left[(K_s)^{-1} \quad i_{qds1}\right]^T \frac{\partial}{\partial \theta_r}L'_{sr1}(K_r)^{-1}i_{qdr} + \\ & p_2\left[(K_s)^{-1} \quad i_{qds2}\right]^T \frac{\partial}{\partial \theta_r}L'_{sr2}(K_r)^{-1}i_{qdr} \end{aligned} \tag{54}$$

In complex vector form, the expression for the total electromagnetic torque is given by

$$T_e = \frac{3}{2}p_1\mathrm{Im}\left[\underline{\lambda}^*_{qds1} \quad \underline{i}_{qds1}\right] + \frac{3}{2}p_2\mathrm{Im}\left[\underline{\lambda}^*_{qds2} \quad \underline{i}_{qds2}\right] \tag{55}$$

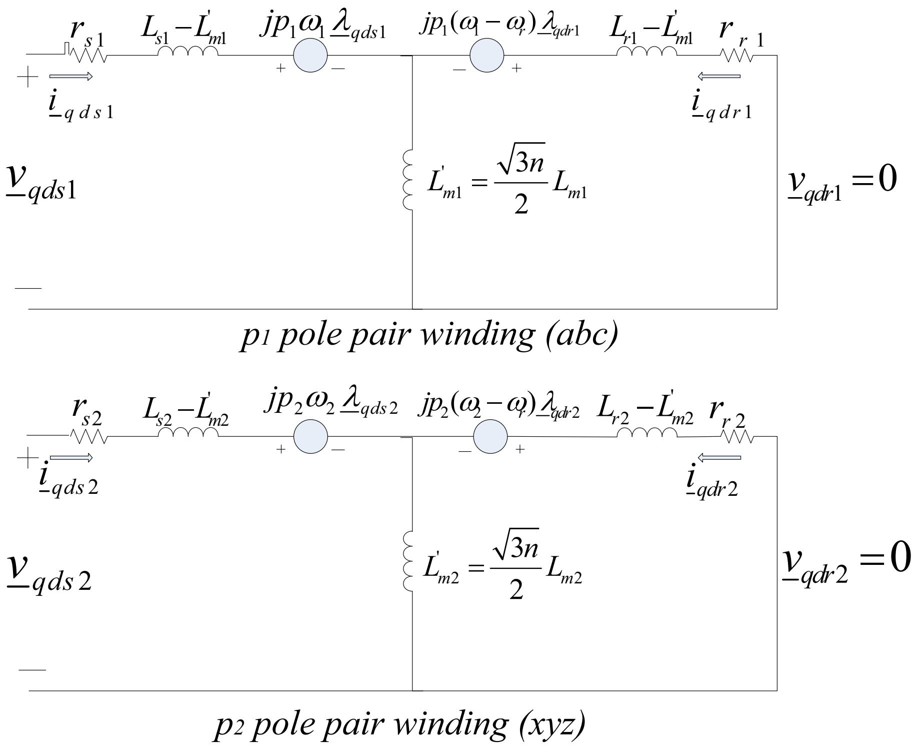

Fig. 2. Complex Vector *qd* Equivalent Circuit.

2.7. Inverse transformation

The inverse transformation for the *abc* and *xyz* stator winding currents is given by [18]:

$$\underline{i}_{s1} = e^{j\theta}\underline{i}_{qds1} \tag{56}$$

$$\underline{i}_{s2} = e^{j\theta}\underline{i}_{qds2} \tag{57}$$

The individual phase currents can thus be obtained as follows:

$$i_{as} = \mathrm{Re}[\underline{i}_{s1}] \tag{58}$$

$$i_{bs} = \mathrm{Re}[\underline{a}\underline{i}_{s1}] \tag{59}$$

$$i_{cs} = \mathrm{Re}[\underline{a}^2\underline{i}_{s1}] \tag{60}$$

The phase currents of *xyz* stator winding can thus be similarly obtained.

Inverse transformation for the rotor currents can be obtained from (40) as follows:

$$\underline{i}_{qdr1} = \frac{2}{3}\sqrt{\frac{3}{n}}e^{-j(\theta_1-\theta_r-\delta)}\underline{i}_{r1} \tag{61}$$

$$\underline{i}_{qdr2} = \frac{2}{3}\sqrt{\frac{3}{n}}e^{-j(\theta_2-\theta_r-\delta)}\underline{i}_{r2} \tag{62}$$

thus,

$$\underline{i}_{r1} = \frac{3}{2}\sqrt{\frac{n}{3}}e^{j(\theta_1-\theta_r-\delta)}\underline{i}_{qdr1} \tag{63}$$

and

$$\underline{i}_{r2} = \frac{3}{2}\sqrt{\frac{n}{3}}e^{j(\theta_2-\theta_r-\delta)}\underline{i}_{qdr2} \tag{64}$$

where

$$\delta = \frac{\alpha_r}{2} = \frac{2\pi/n}{2} = \frac{\pi}{n} \tag{65}$$

Individual loop current i_{ri} can be obtained by

$$i_{ri} = \mathrm{Re}\left[\underline{i}_{r1} \times \underline{b}^{p_1(i-1)}\right] \tag{66}$$

or

$$i_{ri} = \mathrm{Re}\left[\underline{i}_{r2} \times \underline{b}^{p_2(i-1)}\right] \tag{67}$$

Where $\underline{b}$ is already defined from (23).

The *ith* rotor bar current can thus be obtained as follows:

$$i_{rbi} = i_{ri+1} - i_{ri} \tag{68}$$

3. Procedures for the simulation of the dual Stator-winding induction Machine

The equations derived in the previous section are arranged in forms suitable for simulation. A simple modular approach employed by [20] and [21] for induction macine has been modified and applied for complex vector representations suitable for the dual stator winding induction machine. The simulation has been done in the complex vector form using MATLAB-Simulink.

From (45)–(48), the complex vector currents can be written as

$$\underline{i}_{qds1} = \frac{\underline{\lambda}_{qds1} - L'_{m1}\underline{\lambda}_{qdr1}}{L_{s1}} \tag{69}$$

$$\underline{i}_{qds2} = \frac{\underline{\lambda}_{qds2} - L'_{m2}\underline{\lambda}_{qdr2}}{L_{s2}} \tag{70}$$

$$\underline{i}_{qdr1} = \frac{\underline{\lambda}_{qdr1} - L'_{m1}\underline{\lambda}_{qds1}}{L_{r1}} \tag{71}$$

Please cite this article in press as: A.S.O. Ogunjuyigbe et al., Modelling and analysis of dual stator-winding induction machine using complex vector approach, Eng. Sci. Tech., Int. J. (2018), https://doi.org/10.1016/j.jestch.2018.03.013

$$\underline{i}_{qdr2} = \frac{\underline{\lambda}_{qdr2} - L'_{m2}\underline{\lambda}_{qds2}}{L_{r2}} \tag{72}$$

Each current in the LHS of Eqs. (56)–(59) can be expressed in terms of the flux linkages by making substitutions for the other current in the RHS of each equation. Thus,

$$\begin{aligned}\underline{i}_{qds1} &= \frac{L_{r1}}{L_{r1}L_{s1} - L'^2_{m1}}\underline{\lambda}_{qds1} - \frac{L'_{m1}}{L_{r1}L_{s1} - L'^2_{m1}}\underline{\lambda}_{qdr1} \\ &= D_1\left[L_{r1}\underline{\lambda}_{qds1} - L'_{m1}\underline{\lambda}_{qdr1}\right]\end{aligned} \tag{73}$$

$$\begin{aligned}\underline{i}_{qds2} &= \frac{L_{r2}}{L_{r2}L_{s2} - L'^2_{m2}}\underline{\lambda}_{qds2} - \frac{L'_{m2}}{L_{r2}L_{s2} - L'^2_{m2}}\underline{\lambda}_{qdr2} \\ &= D_2\left[L_{r2}\underline{\lambda}_{qds2} - L'_{m2}\underline{\lambda}_{qdr2}\right]\end{aligned} \tag{74}$$

$$\begin{aligned}\underline{i}_{qdr1} &= \frac{L_{s1}}{L_{r1}L_{s1} - L'^2_{m1}}\underline{\lambda}_{qdr1} - \frac{L'_{m1}}{L_{r1}L_{s1} - L'^2_{m1}}\underline{\lambda}_{qds1} \\ &= D_1\left[L_{s1}\underline{\lambda}_{qdr1} - L'_{m1}\underline{\lambda}_{qds1}\right]\end{aligned} \tag{75}$$

$$\begin{aligned}\underline{i}_{qdr2} &= \frac{L_{s2}}{L_{r2}L_{s2} - L'^2_{m2}}\underline{\lambda}_{qdr2} - \frac{L'_{m2}}{L_{r2}L_{s2} - L'^2_{m2}}\underline{\lambda}_{qds2} \\ &= D_2\left[L_{s2}\underline{\lambda}_{qdr2} - L'_{m2}\underline{\lambda}_{qds2}\right]\end{aligned} \tag{76}$$

where

$$D_1 = \frac{1}{L_{r1}L_{s1} - L'^2_{m1}} \tag{77}$$

and

$$D_2 = \frac{1}{L_{r2}L_{s2} - L'^2_{m2}} \tag{78}$$

Upon substitution of (60)–(63) into (41)–(44) respectively with the flux linkages made the subjects in each equation, we have

$$\underline{\lambda}_{qds1} = \int \left(\underline{v}_{qds1} + r_{s1}D_1L'_{m1}\underline{\lambda}_{qdr1} - [r_{s1}D_1L_{r1} + jp_1\omega_1]\underline{\lambda}_{qds1}\right)dt \tag{79}$$

$$\underline{\lambda}_{qds2} = \int \left(\underline{v}_{qds2} + r_{s2}D_2L'_{m2}\underline{\lambda}_{qdr2} - [r_{s2}D_2L_{r2} + jp_2\omega_2]\underline{\lambda}_{qds2}\right)dt \tag{80}$$

$$\underline{\lambda}_{qdr1} = \int \left(\underline{v}_{qdr1} + r_{r1}D_1L'_{m1}\underline{\lambda}_{qds1} - [r_{r1}D_1L_{s1} + jp_1(\omega_1 - \omega_r)]\underline{\lambda}_{qdr1}\right)dt \tag{81}$$

$$\underline{\lambda}_{qdr2} = \int \left(\underline{v}_{qdr2} + r_{r2}D_2L'_{m2}\underline{\lambda}_{qds2} - [r_{r2}D_2L_{s2} + jp_2(\omega_2 - \omega_r)]\underline{\lambda}_{qdr2}\right)dt \tag{82}$$

4. MATLAB-Simulink implementation of the mathematical model

The equatons in the previous sections have been implemented using MATLAB-Simulink. The overall system configuration is shown in Fig. 3.

The model is made up of the different subsystems as shown in Fig. 3. The details in the complex voltage subsystem is shown in Fig. 4. This implements the voltage equations arbitrarily denoted by (38). The source voltage for the *abc* stator winding is shown in Fig. 5, which is a subsystem in the complex voltage subsystem. This is similar to the one for the *xyz* stator winding.

Figs. 6 and 7 respectively shows the internal details of the complex stator flux linkage subsystem named "LamdaQDs" which

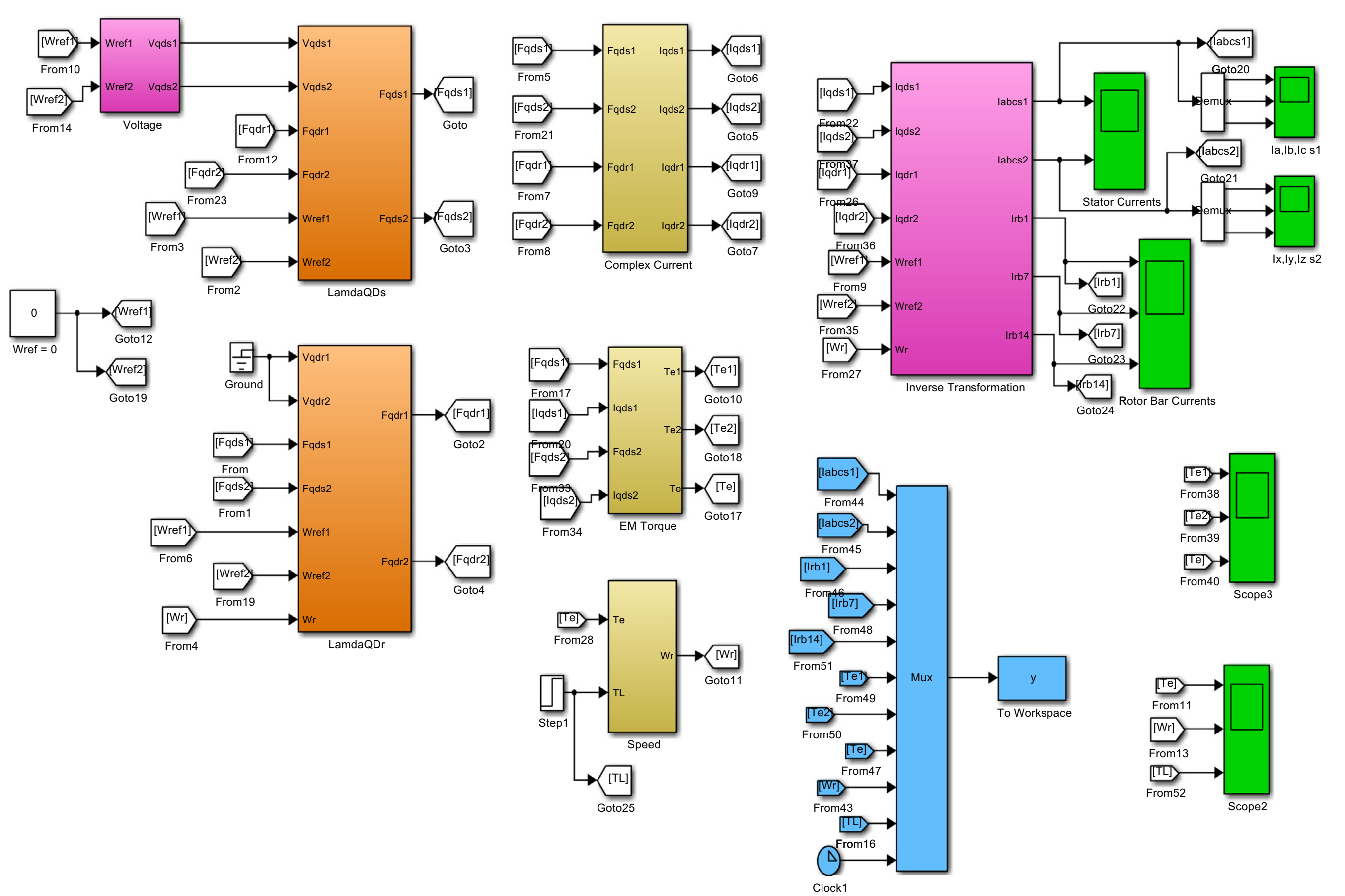

Fig. 3. Simulink Model of Dual Stator Induction Machine.

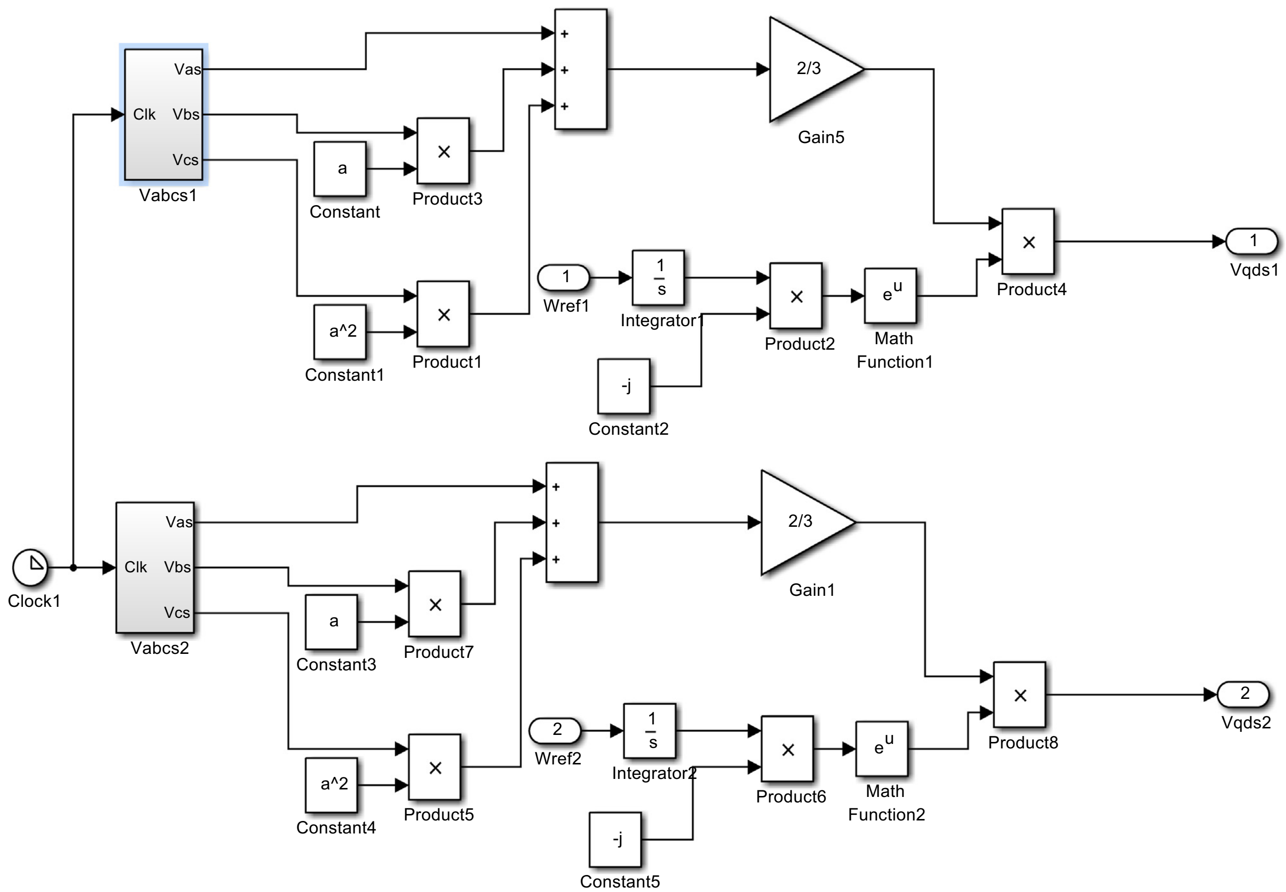

Fig. 4. Complex Voltage Subsystem.

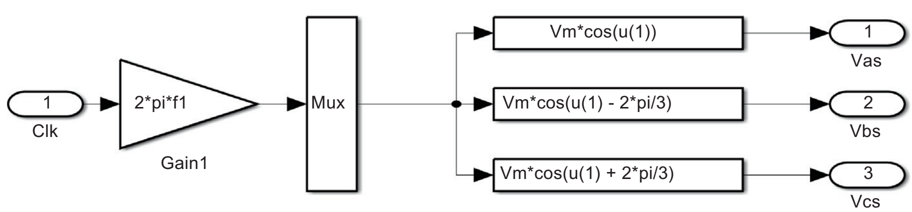

Fig. 5. Source Voltage (abcs) Subsystem.

implements equations (79) and (80) and the complex rotor flux linkage subsystem named "LamdaQDr" which implements Eqs. (81) and (82).

Fig. 8 is the implementation of the complex current equations given by (73)(76).

The inverse transformation subsystem shown in Fig. 9 transforms the *qd* complex vector stator and rotor currents into machine variables. This subsystem implements (56)–(68). The *abc* stator currents and associated rotor currents are obtained from the subsystem in Fig. 10. The details of the second subsystem shown in Fig. 9 for the *xyz* stator current and and associated rotor currents are similar to those shown in Fig. 10. Figs. 11 and 12 shows the subsystem that implements the torque and the speed equations.

5. Simulation results

The computer simulation of the dual stator winding induction machine is presented in this section. The parameters of a conventional 3hp induction machine has been used for both stator windings. The details of the parameters used for the simulation are provided in [7].

Two cases have been analysed. The first case represents the input condition in which both stator windings are motoring, and the second case represents the input condition that allows one of the stator windings (*abc* stator winding) to be in the generating mode and the other (*xyz* stator winding) in the motoring mode. The two cases are analysed in what follows.

5.1. Case 1: Both stator windings are in motoring mode

In the first case, the *abc* stator winding (2-pole) is supplied with a line-to-line voltage of 67 V, 30 Hz supply, and the *xyz* stator winding (6-pole) with a line-to-line voltage of 202 V, 90 Hz supply. This satisfies the constant voltage/hertz condition whereby the ratio of the voltage and frequency of the *abc* stator winding (2-pole) to those of the *xyz* stator winding (6-pole) is 1:3.

Figures 13(i)–(iii) shows the dynamic performances of the machine under this supply condition. The no load dynamic perfor-

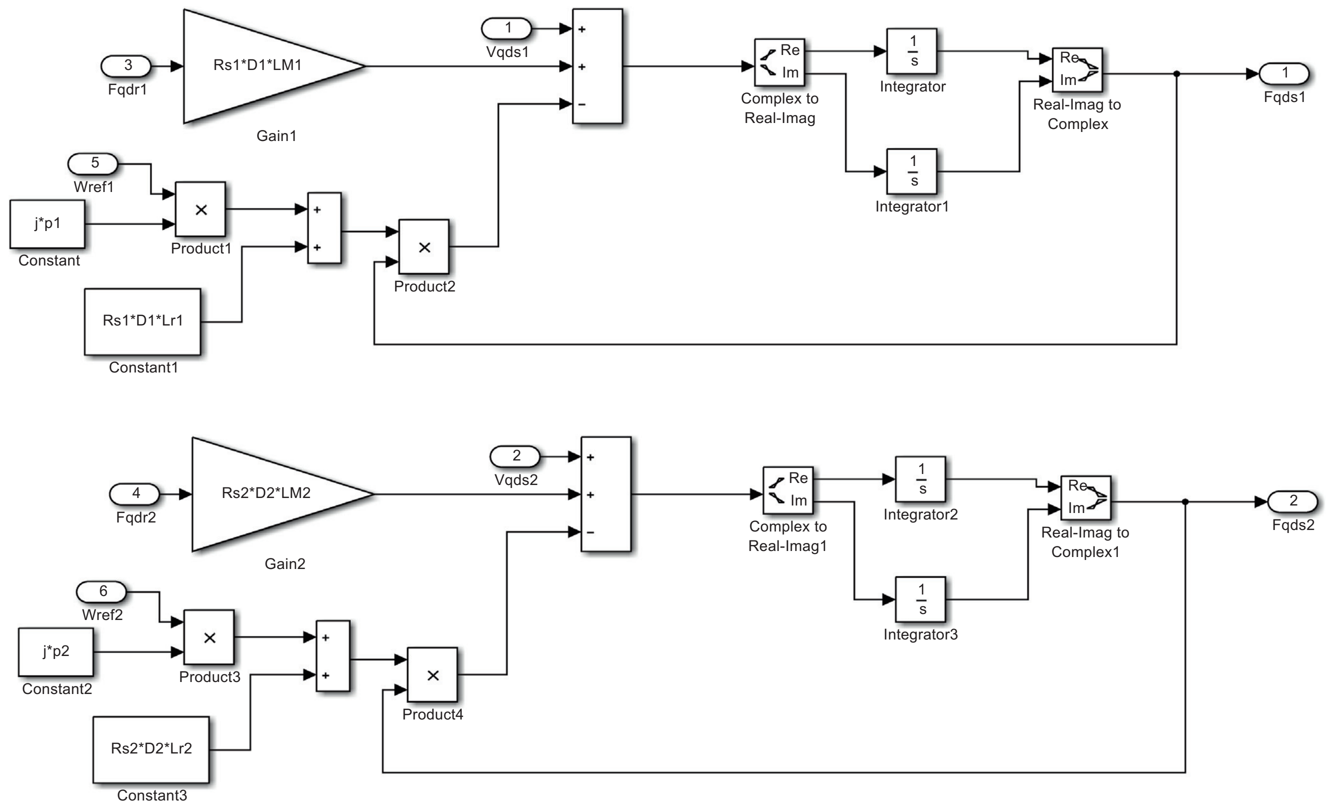

Fig. 6. Complex Stator Flux Linkage Subsystem (LamdaQDs) Subsystem.

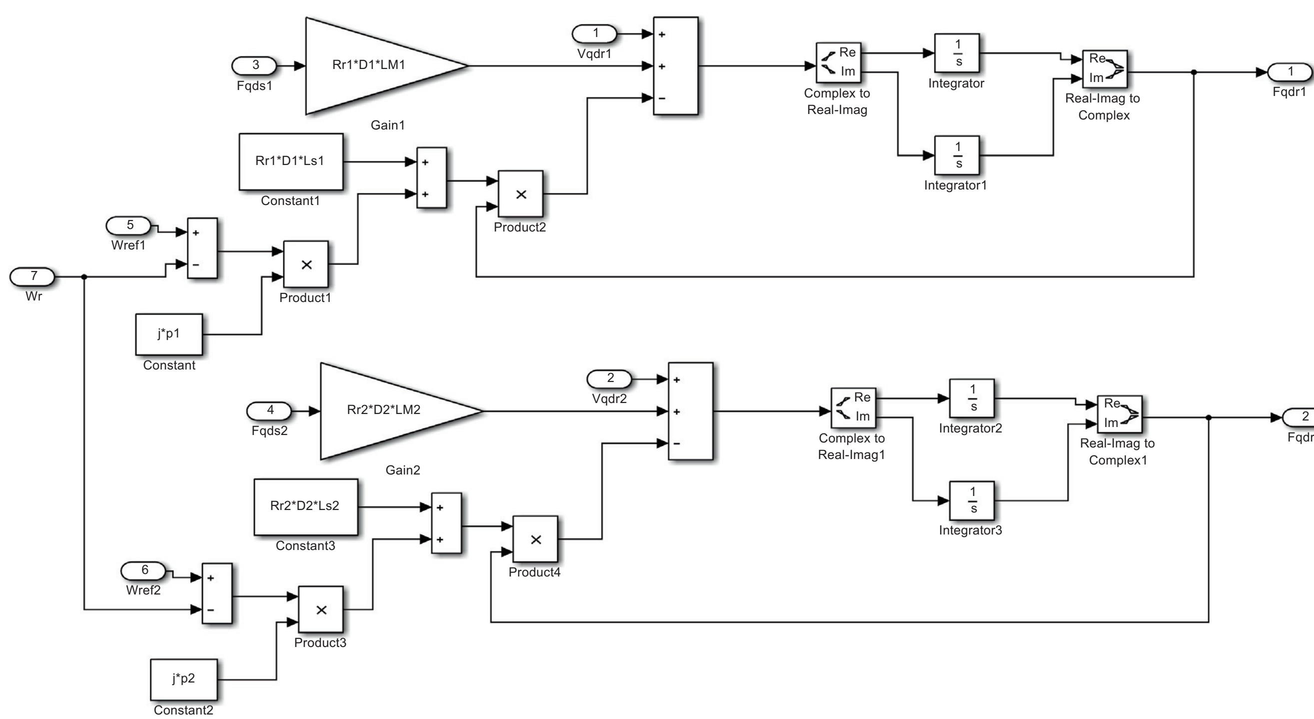

Fig. 7. Complex Rotor Flux Linkage Subsystem (LamdaQDr) Subsystem.

mances are shown from 0 to 0.4 s, after which a constant load torque of 20Nm was applied. The dynamic response of the machine under the 20Nm load is shown from 0.4 to 1 s. It can be observed from the Figure traces that there is a smooth starting process. A high starting current for both stator windings and the rotor bars, with the *xyz* stator winding current about two times higher than the *abc* stator winding current. The starting current in the rotor bar could be very high, but which quickly falls to zero at about

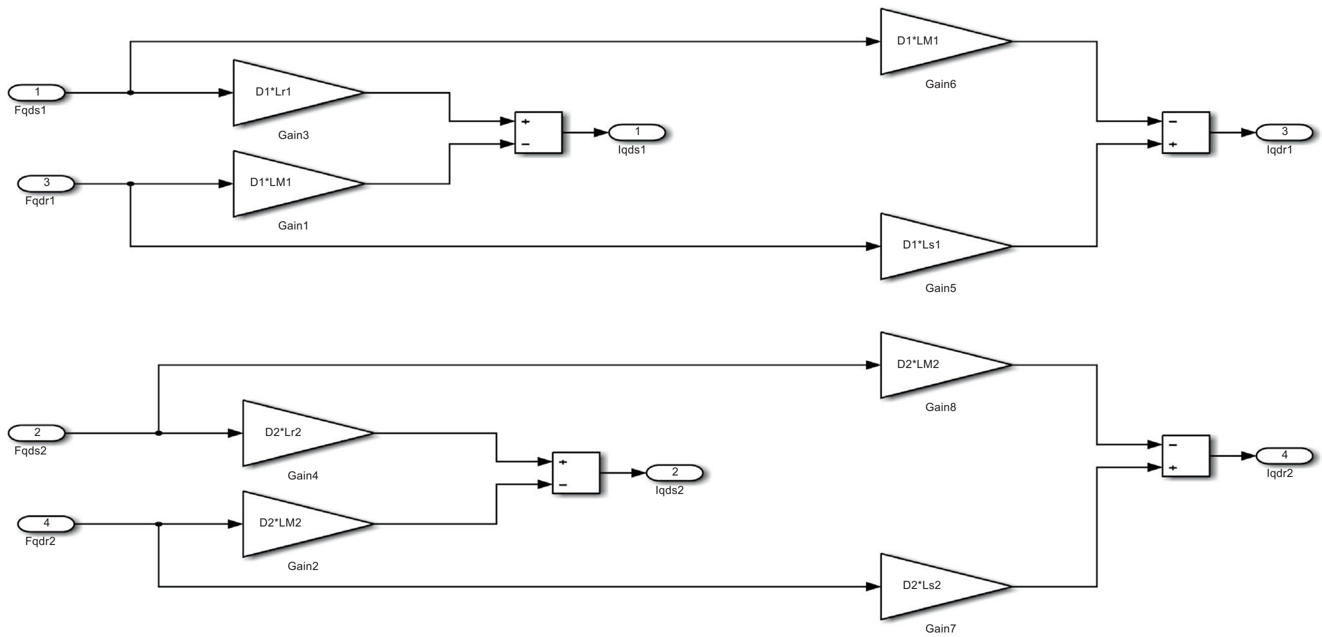

Fig. 8. Complex Current Subsystem.

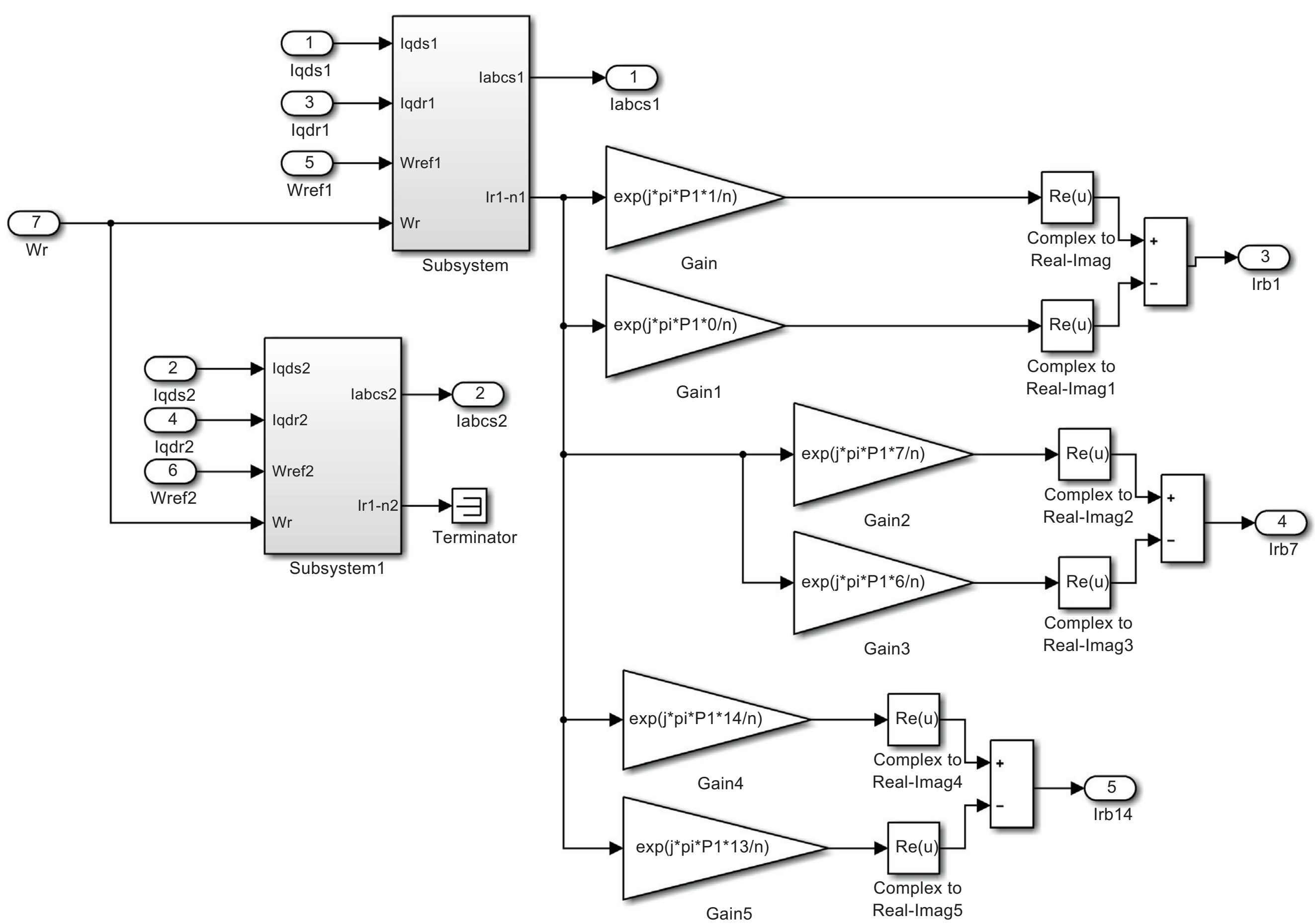

Fig. 9. Inverse Transformation Subsystem.

0.2 s during the no load condition which lasts up to 0.4 s. The rotor speed rises up to about 186 rad/s during the no load transient and then falls to 175 rad/s after the 20Nm load is applied.

It can also be observed that the torque contribution of the *abc* stator winding (2-pole) is very small (4 Nm at steady state) compared to that of the *xyz* stator winding (6-pole) which supplies

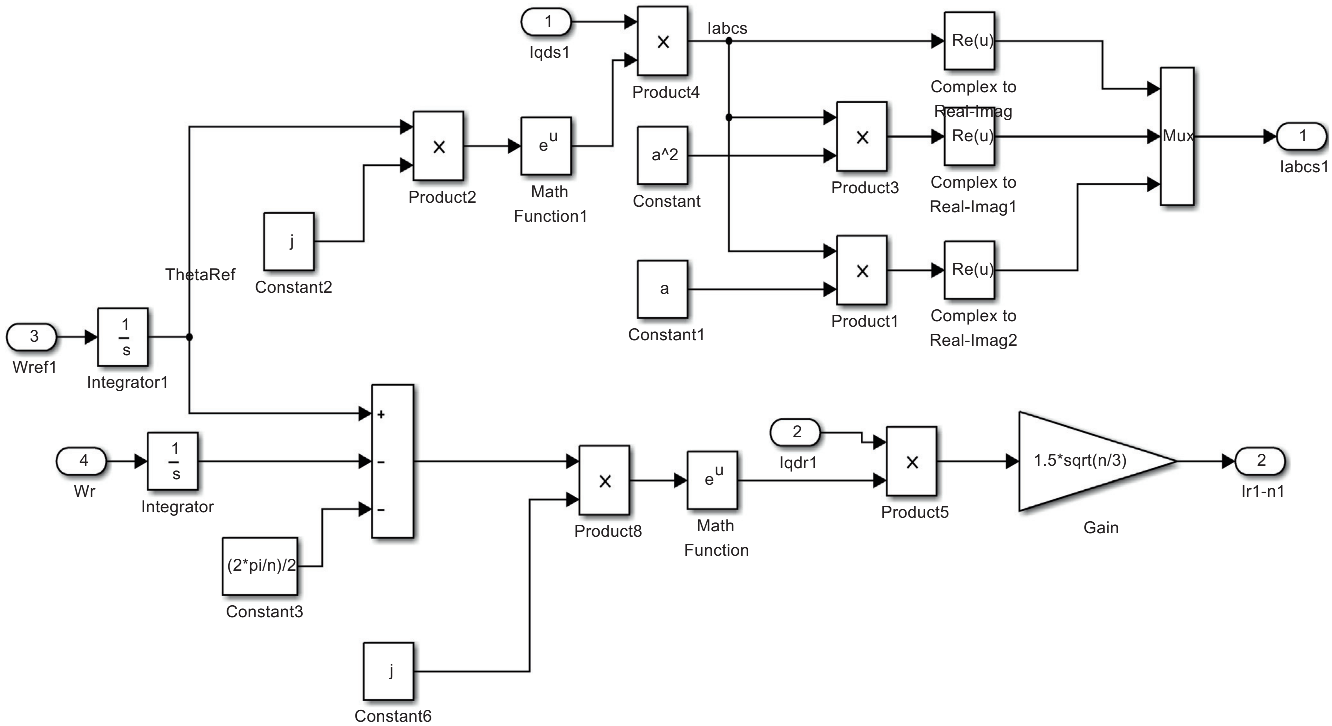

Fig. 10. *abc* stator current and rotor currents Subsystem.

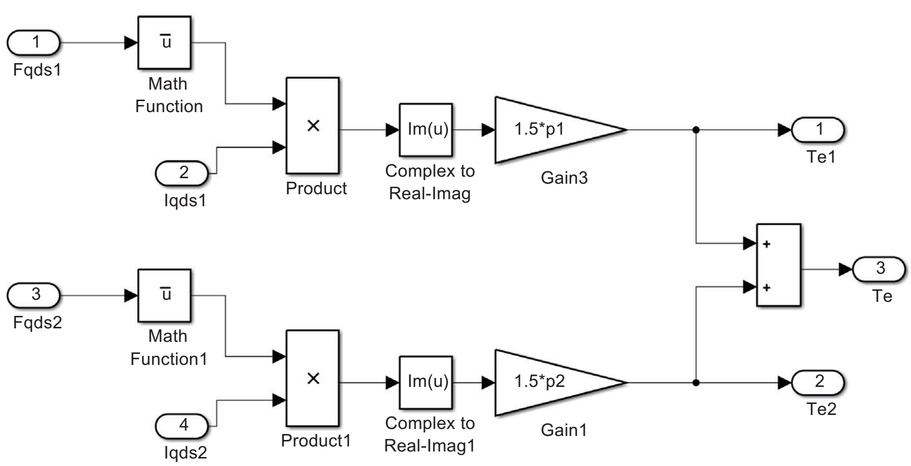

Fig. 11. Electromagnetic Torque Subsystem.

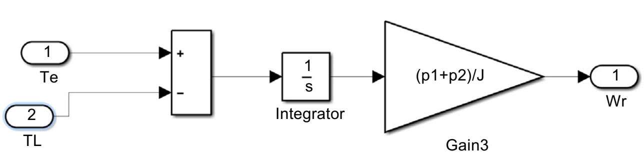

Fig. 12. Rotor Speed Subsystem.

most of the electromagnetic torque (16 Nm at steady state), both of which adds up to meet the load demand of 20Nm. However, the two torques can be controlled based on the input control conditions such that the *abc* stator winding can produce a larger torque or even a negative torque, in which case its winding is in the generating mode.

5.2. Case 2: Abc stator winding in generating mode & xyz stator winding in motoring mode

In this case, the *abc* stator winding (2-pole) is made to operate in the generating mode by changing the input conditions specified in the first case. The frequency of the *abc* stator winding (2-pole) is changed to 20 Hz, while other input conditions remain unchanged. Figures 14(i)–(iii) shows the dynamic performances of the machine under this case. The no load dynamic performances are shown from 0 to 0.4 s, after which a constant load torque of 20Nm was applied. The dynamic response of the machine under the 20Nm load is shown from 0.4 to 1 s. The rotor speed rises up to about 170 rad/s during the no load transient and then falls to 155 rad/s after the 20 Nm load is applied.

It can be observed that the electromagnetic torque developed by the *abc* stator winding (2-pole) is negative (-11.6 Nm at steady

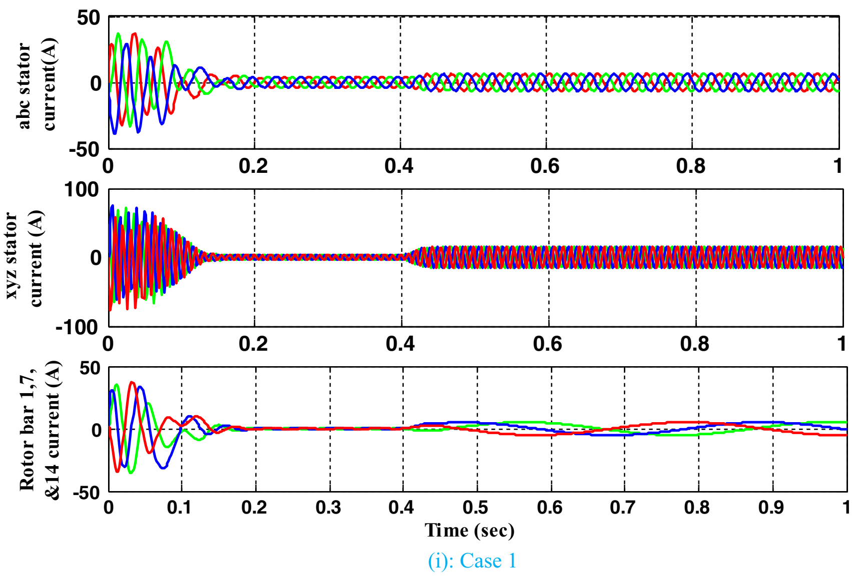

Fig. 13i. Case 1.

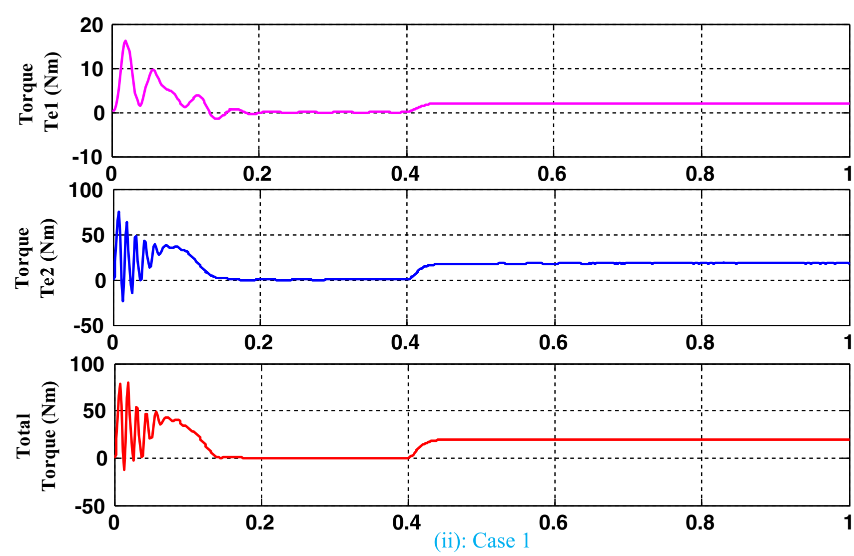

Fig. 13ii. Case 1.

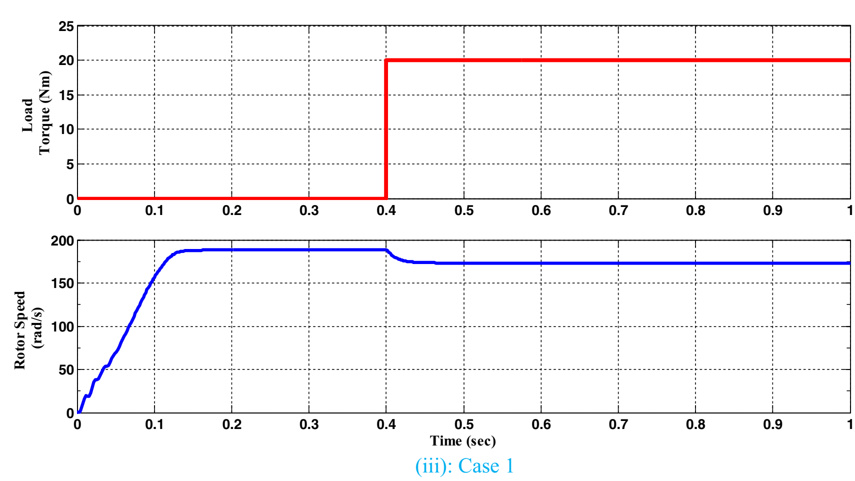

Fig. 13iii. Case 1.

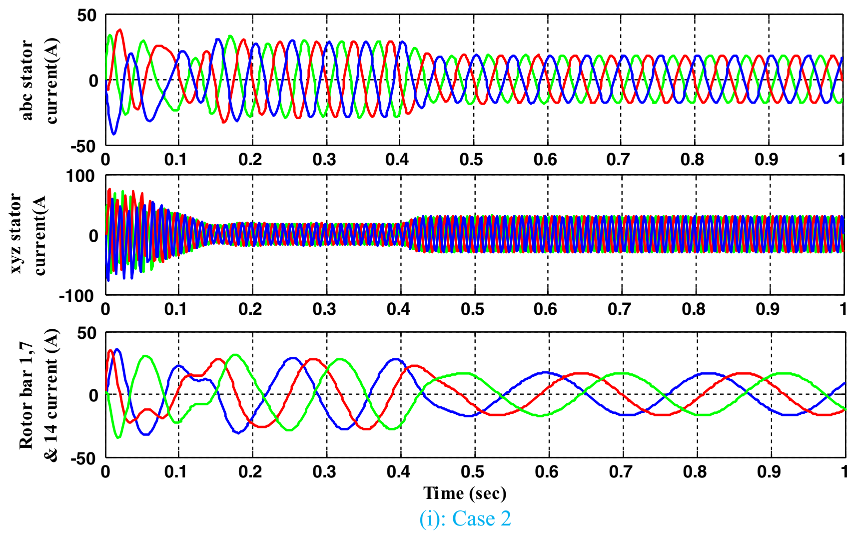

Fig. 14i. Case 2.

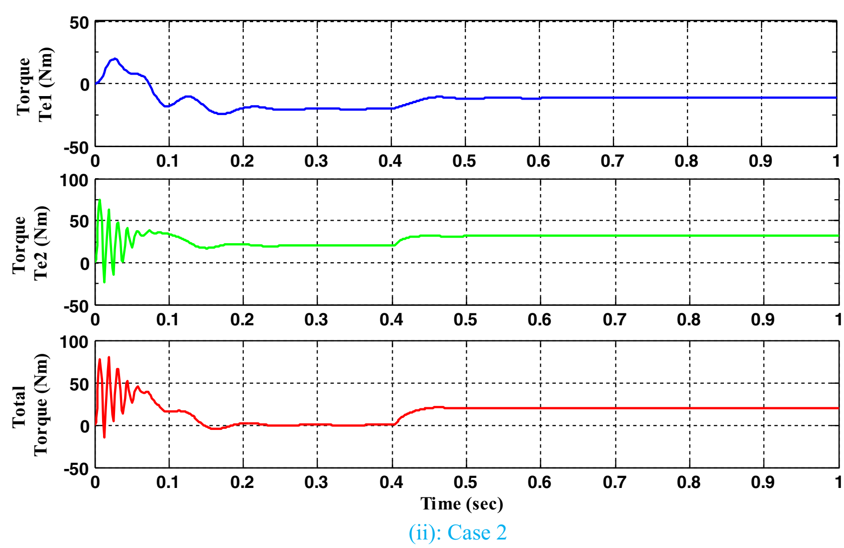

Fig. 14ii. Case 2.

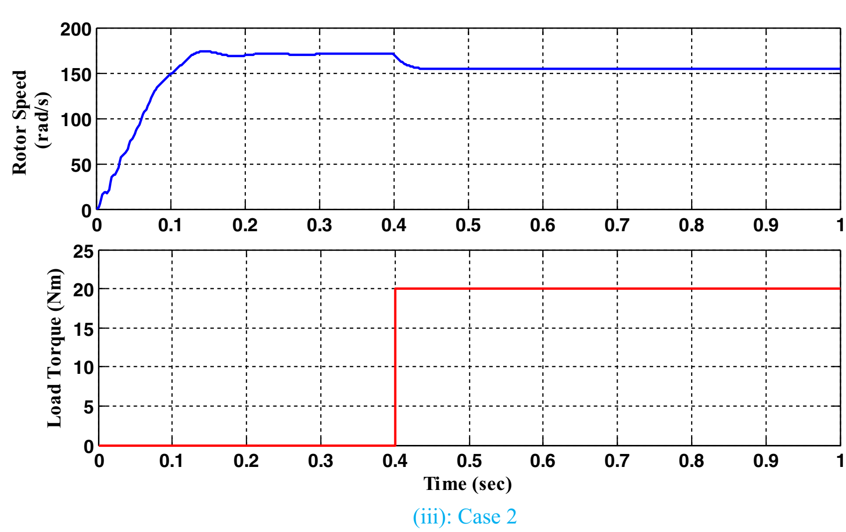

Fig. 14iii. Case 2.

Please cite this article in press as: A.S.O. Ogunjuyigbe et al., Modelling and analysis of dual stator-winding induction machine using complex vector approach, Eng. Sci. Tech., Int. J. (2018), https://doi.org/10.1016/j.jestch.2018.03.013

state) and that developed by the *xyz* stator winding (6-pole) is positive (31.6 Nm at steady state), which has to account for the negative torque of the *abc* stator winding and the load torque.

It is clearly seen that under this case, the *abc* stator winding is generating while the *xyz* stator winding is motoring. This is a significant advantage of the dual stator winding induction machine whereby any mode of machine operation (motoring or generating) mode can be achieved by the input or control conditions. The simulation results obtained in this work is very similar to those obtained in [5].

6. Conclusion

Modelling and simulation of the dual stator winding induction machine with squirrel-cage rotor has been presented. The dynamic performance of the machine has been analysed under two sets of input conditions, whereby in the first case both stator windings are motoring while in the second case, one of the stator windings is motoring while the other is generating. A step-by-step procedure for the MATLAB-Simulink model has been clearly presented which could enhanced the understanding of complex vector application in modelling and simulation of electrical machines. The results presented in this work are in agreement with the results in [5] which confirms the accuracy and robustness of the results. This work demonstrates the usefulness of complex vector approach for modelling and simulation of induction machine in MATLAB-Simulink. The approach presented in this work can easily be applied to other types and configurations of electric machines and drives.

Conflict of interest

The authors declare that there is no any conflicting of interest concerning the publication of this manuscript

References

[1] J. Poza, E. Oyarbide, D. Roye, M. Rodriguez, Unified reference frame dq model of the brushlessdoubly fed machine, IEE Proc. Electric Power Appl. 153 (2006).

[2] S. Basak, C. Chakraborty, Dual Stator Winding Induction Machine: Problems, Progress, and Future Scope, IEEE Trans. Ind. Electr. 62 (2015) 4641–4652.

[3] C. Wang, K. Wang, X. You, Research on Synchronized SVPWM Strategies Under Low Switching Frequency for Six-Phase VSI-Fed Asymmetrical Dual Stator Induction Machine, IEEE Trans. Ind. Electr. 63 (2016) 6767–6776.

[4] W. Kun, Y. Xiaojie, W. Chenchen, Z. Minglei, "An equivalent dual three-phase SVPWM realization of the modified 24-sector SVPWM strategy for asymmetrical dual stator induction machine," in, IEEE Energy Convers. Congr. Exposition (ECCE) 2016 (2016) 1–7.

[5] Z. Wu, O. Ojo, Coupled-circuit-model simulation and airgap-field calculation of a dual-stator-winding induction machine, IEE Proc. Electr. Power Appl. 153 (2006) 387–400.

[6] A.R. Munoz, T.A. Lipo, Dual stator winding induction machine drive, IEEE Trans. Ind. Appl. 36 (2000) 1369–1379.

[7] P. Krause, O. Wasynczuck, S. Sudhoff, Analysis of Electric Machinery and Drive System, John Wiley & Son Publication, 2002.

[8] K. Pienkowski, Analysis and Control of Dual Stator Winding Induction Motor, Arch. Electr. Eng. 61 (2012) 421–438.

[9] A.R. Dehghanzadeh, V. Behjat, Dynamic Modelling and Experimental Validation of a Dual Stator PMSG for Low Speed Applications, Gazi Univ. J. Sci. 28 (2015) 275–283.

[10] F. Bu, Y. Hu, W. Huang, K. Shi, Control and Implementation of Dual-Stator-Winding Induction Generator for Variable Frequency AC-Generating System, J. Power Electr. 13 (2013) 798–805.

[11] M.B. Slimene, M.A. Khlifi, M. Benfredj, H. Rehaoulia, Double Stator Induction Generator Model for Autonomous Operating Mode, World Appl. Sci. J. 30 (2014) 1370–1375.

[12] M.B. Slimene, M.A. Khlifi, M. Benfredj, H. Rehaoulia, Self Excitation in Dual Stator Winding Induction Generator for Renewable Energy Generation, in: The fifth International Renewable Energy Congress, Hammamet, TUNISIA, pp. 1–5.

[13] J.A.B. Rodrigo, X.M. Puig, H.V. Blavi, L.G. Pesquer, Implementation, Modelling and Performance Analysis of a Dual Stator-Winding Induction Generator, Int. J. Comput. Math. Electr. Electr. Eng. 32 (2013) 302–312.

[14] H. Amimeur, R. Abdessemed, D. Aouzellag, E. Merabet, F. Hamoudi, Modeling and Analysis of Dual-Stator Windings Self-Excited Induction Generator, J. Electr. Eng. 6 (2015) 1–6.

[15] F. Hamoud, M.L. Doumbia, A. Cheriti, Performance Study of a Self-Excitation Dual Stator Winding Induction Generator for Renewable Distributed Generation Systems, Smart Grid Renew. Energy 7 (2016) 197–215.

[16] A.R. Munoz, T.A. Lipo, Complex variable model of the squirrel cage induction machine including instantaneous rotor bar current, IEEE Trans. Ind. Appl. (1999) 1332–1340.

[17] A.J.S. Filho, E.R. Filho, The complex controller for three-phase induction motor direct torque control, Sba: Controle & Automação Sociedade Brasileira de Automatica 20 (2009) 256–262.

[18] D.W. Novotny, T.A. Lipo, Vector control and dynamics of AC drives, Clarendon Press, Oxford, 1996.

[19] A.R. Munoz, T.A. Lipo, Complex variable model of the squirrel cage induction machine including instantaneous rotor bar current, IEEE Trans. Ind. Appl. (1999) 1332–1340.

[20] B. Ozpineci, L.M. Tolbert, Simulink Implementation of Induction Machine Model-A Modular Approach, in: Proceedings of the IEEE International Electric Machines and Drives Conference (IEMDC), ed, 2003, pp. 728–734.

[21] A.W. Leedy, Simulink / MATLAB Dynamic Induction Motor Model for Use as a Teaching and Research Tool, Int. J. Soft Comput. Eng. (IJSCE) 3 (2013) 102–107.

Please cite this article in press as: A.S.O. Ogunjuyigbe et al., Modelling and analysis of dual stator-winding induction machine using complex vector approach, Eng. Sci. Tech., Int. J. (2018), https://doi.org/10.1016/j.jestch.2018.03.013